A Letters Journal Exploring the Frontiers of Physics

January 2018

EPL, **121** (2018) 24002
doi: 10.1209/0295-5075/121/24002

www.epljournal.org

Microfluidic flow actuation using magnetoactive suspensions

R. Alonso-Matilla and D. Saintillan[(a)]

Department of Mechanical and Aerospace Engineering, University of California San Diego 9500 Gilman Drive, La Jolla, CA 92093, USA

received 11 January 2018; accepted in final form 27 February 2018
published online 19 March 2018

PACS 47.57.Qk – Complex fluids and colloidal systems: Rheological aspects
PACS 47.63.Gd – Swimming microorganisms
PACS 47.65.Cb – Magnetic fluids and ferrofluids

Abstract – The rheological behavior of magnetotactic bacterial suspensions is analyzed using a continuum kinetic theory. In both unbounded and confined geometries, the response of these suspensions under simple external flows can be controlled by applying a magnetic field and hinges in a subtle way on the interplay of magnetic alignment, rotation under shear, and wall-induced accumulation under confinement. By tuning magnetic field strength and direction, the apparent viscosity can either be enhanced or reduced, and the mechanisms for these trends are elucidated. In the absence of any applied flow, we further demonstrate the ability of magnetoactive suspensions to internally drive steady unidirectional flows upon application of a magnetic field, thus suggesting novel avenues for the design of microfluidic pumps and flow actuation devices.

Introduction. – Suspensions of active particles, such as motile microorganisms, synthetic microswimmers, or externally actuated colloids, exhibit unusual rheological properties that are unlike those of classical complex fluids [1]. While the additional viscous dissipation incurred by flow around suspended particles typically enhances viscosity in passive systems [2], such is not the case in active suspensions, where mechanical stresses generated on the microscale as a result of activity can have the opposite effect of reducing flow resistance [3]. This curious trend has been characterized in detail in the case of swimming bacteria [4,5], where the coupling of particle reorientations by the applied flow and of dipolar stresses exerted during self-propulsion indeed causes a decrease in viscosity in weak flows [6]. In sufficiently concentrated systems, the apparent viscosity can in fact reach zero [5,7], indicating a transition to a superfluid-like state where internal activity exactly compensates viscous dissipation. A dramatic manifestation of this transition is the emergence of spontaneous directed motions in confined systems [8,9], which has been explained as a linear instability driven by active stresses [10]. The ability to harness these flows for applications, however, remains limited due to the lack of external control on particle configurations, which instead emerge spontaneously from internal mechanical couplings.

Tunable rheological properties are typically achieved in passive systems by applying external electric or magnetic fields [11,12], which drive particle rearrangements or reorientations and thus affect resistance to flow. The viscous properties of passive magnetic fluids have been extensively studied, with experiments [13] showing an increase in the viscosity of ferromagnetic fluids when a constant magnetic field is applied. This effect is well understood theoretically [14–18] as a consequence of the magnetic torque acting on the particles, which hinders their rotation by the applied vorticity and results in an additional stress contribution.

In this work, we investigate the use of magnetic fields as a means to control the effective rheology and internally-driven flows of active suspensions in microfluidic channels. The system of choice for this problem is magnetotactic bacteria, which are motile prokaryotes mostly present in marine habitats that synthesize intracellular magnetic membrane-bound crystals known as magnetosomes. These bacteria, which swim by similar mechanisms as other flagellated bacteria, behave as self-propelled permanent magnetic dipoles that orient and migrate along the local magnetic field lines [19]. Magnetotactic suspensions thus behave as magnetic fluids with additional complexities arising from self-propulsion, which causes particle accumulation at walls in confined systems [20,21], and from active stresses, which modify the rheology [1,6,7]. Although the

[(a)] E-mail: dstn@ucsd.edu

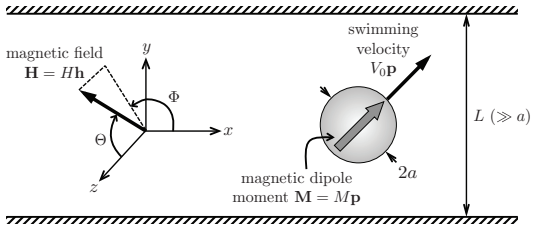

Fig. 1: Problem definition: a dilute suspension of spherical magnetotactic swimmers (velocity $V_0\mathbf{p}$, magnetic dipole $\mathbf{M} = M\mathbf{p}$) is subject to an externally applied magnetic field $\mathbf{H}$.

active nature of magnetotactic bacteria has not been characterized in detail experimentally, it has been suggested that the strain MC-1 of *Magnetococcus marinus* behaves as a puller [22]. The ability to manufacture magnetotactic pusher-like particles using engineered flagellar motors of *Escherichia coli* bacteria tethered to magnetic beads has also been demonstrated [23].

The complex dynamics of magnetoactive suspensions in microfluidic flows have recently been studied in experiments [22], where the interplay of magnetic alignment and rotation in shear was shown to cause flow-focusing in pressure-driven flow [24]. In semi-dilute systems, a pearling instability was observed [22], though it remains unclear whether it is caused by hydrodynamic [25] or magnetic [26] interactions. These experiments hint at an unusual rheology, which we analyze in this letter. We show that, when placed in an external uniform magnetic field, a confined magnetotactic suspension can behave as an active ferromagnetic pump. When the direction of the field and the magnetization of the microorganisms are not collinear, bacteria feel a net magnetic torque which is transmitted to the surrounding fluid, and can give rise to a net unidirectional fluid flow in a planar channel, with a flow rate and direction that can be controlled by adjusting both the magnitude and orientation of the field. Using a kinetic theory [6,7], we provide a physical explanation for these flows and also analyze the rheological response of magnetotactic suspensions under steady applied flows.

Continuum kinetic model. – We consider a suspension of rigid spherical magnetotactic motile bacteria of radius a dispersed in an incompressible Newtonian solvent with dynamic viscosity η_s. The suspension is assumed to be dilute, with mean number density n and corresponding volume fraction $\phi_v = \frac{4}{3}\pi a^3 n \ll 1$. We study both unbounded and confined systems, where the confining geometry is a Hele-Shaw cell comprised of two infinite parallel plates separated by a distance $L \gg a$. We adopt the coordinate system shown in fig. 1, where x is the flow direction, y the wall-normal coordinate, and z the vorticity direction. A spatially uniform magnetic field $\mathbf{H} = H\mathbf{h}$ is applied along the unit vector $\mathbf{h}$, which we parametrize in spherical coordinates as $\mathbf{h} = (\sin\Theta\cos\Phi, \sin\Theta\sin\Phi, \cos\Theta)$. Bacteria are assumed to swim at constant speed V_0 along their unit director $\mathbf{p}$, similarly expressed as $\mathbf{p} = (\sin\theta\cos\varphi, \sin\theta\sin\varphi, \cos\theta)$. They carry a permanent magnetic dipole modeling the presence of the magnetosome chains that longitudinally traverse the cell body of magnetobacteria [27]: $\mathbf{M} = M\mathbf{p}$. We neglect induced polarization and magnetic interactions and thus assume that $\mathbf{M}$ is constant and rotates rigidly with each cell body. When placed in a uniform external field, the bacteria are subject to a net magnetic torque $\mathbf{M}\times\mathbf{H}$ that generates an additional suspension stress.

Fokker-Planck description. Following previous kinetic models for dilute active fluids [6,7,20,28,29], we describe the configuration of the suspension in terms of the probability density function $\Psi(\mathbf{x},\mathbf{p},t)$ of finding a particle at position $\mathbf{x}$ with orientation $\mathbf{p}$ at time t, where the mean value of Ψ over all positions and orientations defines the number density. At steady state, the density function satisfies the Fokker-Planck equation [30]

$$\nabla_x\cdot(\dot{\mathbf{x}}\Psi) + \nabla_p\cdot(\dot{\mathbf{p}}\Psi) = 0, \tag{1}$$

where $\dot{\mathbf{x}}$ and $\dot{\mathbf{p}}$ capture translational and rotational particle fluxes, respectively. The translational flux is obtained from a force balance on a swimmer,

$$6\pi\eta_s a\left[\dot{\mathbf{x}} - V_0\mathbf{p} - \mathbf{u}(\mathbf{x})\right] + k_\mathrm{B}T\nabla_x\ln\Psi = \mathbf{0}, \tag{2}$$

where the viscous drag force on the spherical particle balances the Brownian force scaling with thermal energy $k_\mathrm{B}T$. In writing eq. (2), we have used the fact that $a \ll L$, so that advection of the particle by the flow simply occurs with the local fluid velocity $\mathbf{u}(\mathbf{x})$ [31]. Introducing the translational diffusivity $d_t = k_\mathrm{B}T/6\pi\eta_s a$, eq. (2) yields

$$\dot{\mathbf{x}} = V_0\mathbf{p} + \mathbf{u}(\mathbf{x}) - d_t\nabla_x\ln\Psi. \tag{3}$$

Similarly, we obtain the rotational flux from an angular momentum balance, where the viscous, magnetic, and Brownian torques on a swimmer sum up to zero:

$$8\pi\eta_s a^3\left[\frac{1}{2}\boldsymbol{\omega}(\mathbf{x}) - \boldsymbol{\Omega}\right] + \mathbf{M}\times\mathbf{H} - k_\mathrm{B}T\mathbf{p}\times\nabla_p\ln\Psi = \mathbf{0}. \tag{4}$$

Here, $\boldsymbol{\omega}(\mathbf{x}) = \nabla_x\times\mathbf{u}(\mathbf{x})$ is the ambient fluid vorticity, while $\boldsymbol{\Omega}$ denotes the bacterium angular velocity. Using the kinematic relation $\dot{\mathbf{p}} = \boldsymbol{\Omega}\times\mathbf{p}$, eq. (4) provides an expression for the rotational flux,

$$\dot{\mathbf{p}} = \frac{1}{2}\boldsymbol{\omega}(\mathbf{x})\times\mathbf{p} + \frac{MH}{8\pi\eta_s a^3}\mathbf{h}^\perp - d_r\nabla_p\ln\Psi, \tag{5}$$

where $d_r = k_\mathrm{B}T/8\pi\eta_s a^3$ is the rotational diffusivity of a spherical particle, and $\mathbf{h}^\perp \equiv (\mathbf{I}-\mathbf{pp})\cdot\mathbf{h}$.

Fluid flow and suspension stress. The suspension of bacteria exchanges both linear and angular momentum with its surroundings, thus affecting the rheology of the system. In the low-Reynolds-number limit relevant to microscopic swimmers, the fluid velocity $\mathbf{u}$ and corresponding pressure q satisfy the incompressible Stokes equations:

$$\nabla_x\cdot\mathbf{u} = 0, \qquad -\nabla_x q + \nabla_x\cdot\boldsymbol{\Sigma} = \mathbf{0}, \tag{6}$$

where the deviatoric stress $\boldsymbol{\Sigma}$ includes contributions from the solvent as well as from the particles. Following

standard methods [1,6,7,14,32], we model the stress as

$$\boldsymbol{\Sigma} = 2\eta_s \left(1 + \frac{10}{3}\pi a^3 c\right)\mathbf{E} + \frac{1}{2}MH\left(\mathbf{hm} - \mathbf{mh}\right) + \sigma_0 \mathbf{D}, \tag{7}$$

where $\mathbf{E} = \frac{1}{2}(\nabla_x \mathbf{u} + \nabla_x \mathbf{u}^T)$ is the rate-of-strain tensor, and c, $\mathbf{m}$ and $\mathbf{D}$ denote the zeroth, first, and second orientational moments of the distribution function:

$$c(\mathbf{x}) = \langle 1 \rangle, \quad \mathbf{m}(\mathbf{x}) = \langle \mathbf{p} \rangle, \quad \mathbf{D}(\mathbf{x}) = \langle \mathbf{pp} - \mathbf{I}/3 \rangle, \tag{8}$$

where $\langle \cdot \rangle = \int \cdot\, \Psi(\mathbf{x}, \mathbf{p})\, \mathrm{d}\mathbf{p}$ is the orientational average. Upon normalization by c, the two moments $\mathbf{m}$ and $\mathbf{D}$ describe local polar and nematic alignment, respectively.

The first term in eq. (7) is a viscous contribution arising from the flow, and involves the usual Newtonian stress corrected for particle concentration according to Einstein's formula [2]. The second term, which is antisymmetric, captures the effect of magnetic torques and vanishes for a suspension aligned with the applied field ($\mathbf{m} \propto \mathbf{h}$) [14,33,34]. Finally, the last term accounts for active stresses arising from self-propulsion and involves the active stresslet σ_0, whose sign depends on the propulsion mechanism [1,3,6]: $\sigma_0 < 0$ for so-called *pusher* swimmers, whereas $\sigma_0 > 0$ for *pullers*. While σ_0 has been measured for certain types of microorganisms [35,36], it is still unknown for common magnetotactic bacteria.

Dimensional analysis. We nondimensionalize the governing equations using time scale d_r^{-1}, length scale L, velocity scale Ld_r, and pressure scale $\eta_s d_r$. The distribution function Ψ is normalized by the number density n. In addition to the volume fraction ϕ_v, scaling of the equations in the absence of an external flow yields four independent dimensionless groups, which we define as

$$\mathrm{Pe}_s = \frac{V_0}{Ld_r}, \quad \epsilon = \frac{\sqrt{d_t/d_r}}{L}, \quad \alpha = \frac{\sigma_0}{k_\mathrm{B}T}, \quad \beta = \frac{MH}{k_\mathrm{B}T}. \tag{9}$$

The swimming Péclet number Pe_s represents the ratio of the persistence length $\ell = V_0/d_r$ of swimmer trajectories over the channel width L, and can be viewed as a measure of confinement. The parameter ϵ is the ratio of the diffusive length scale $\delta = \sqrt{d_t/d_r}$ over L; for a Brownian spherical particle, $\delta = \sqrt{4/3}\,a$, so that $\epsilon \ll 1$ for the case of interest where $a \ll L$. Finally, α and β compare the magnitudes of active and magnetic stresses to the thermal energy unit $k_\mathrm{B}T$. With these scalings, the steady Fokker-Planck eq. (1) simplifies to

$$\begin{aligned} &\nabla_x \cdot \left[\left(\mathrm{Pe}_s \mathbf{p} + \mathbf{u}\right)\Psi\right] - \epsilon^2 \nabla_x^2 \Psi \\ &+ \nabla_p \cdot \left[\left(\frac{1}{2}\boldsymbol{\omega} \times \mathbf{p} + \beta \mathbf{h}^\perp\right)\Psi\right] - \nabla_p^2 \Psi = 0, \end{aligned} \tag{10}$$

subject to a no-flux boundary condition at domain boundaries: $\hat{\mathbf{n}} \cdot (\mathrm{Pe}_s \mathbf{p}\Psi - \epsilon^2 \nabla_x \Psi) = 0$. The scaling of translational diffusion with ϵ^2 underscores the weak role it plays in moderately wide channels outside of near-wall accumulation layers [20]. Similarly, the dimensionless linear momentum conservation equation becomes

$$\begin{aligned} &-\nabla_x q + \left(1 + \frac{5}{2}\phi_v c\right)\nabla_x^2 \mathbf{u} + 5\phi_v \mathbf{E} \cdot \nabla_x c \\ &+ 6\alpha\phi_v \nabla_x \cdot \mathbf{D} + 3\beta\phi_v \left[\mathbf{h} \cdot \nabla_x \mathbf{m} - (\nabla_x \cdot \mathbf{m})\,\mathbf{h}\right] = \mathbf{0}, \end{aligned} \tag{11}$$

where the linear dependence of particle stresses on ϕ_v in the dilute limit is apparent. In the event that an external flow is applied to the system, we also introduce a flow Péclet number defined as $\mathrm{Pe}_f = \dot{\gamma}/d_r$ in an imposed shear flow with shear rate $\dot{\gamma}$, and as $\mathrm{Pe}_f = \Delta q L/\eta_s d_r$ in a pressure-driven flow with pressure gradient Δq.

Results and discussion. – The governing equations (10), (11) are solved numerically using a finite-volume algorithm described in our previous work [7,20]. In unbounded domains, we further check our results using a spectral method based on spherical harmonics [6]. In all results shown here, we assume that the magnetic field lies in the x-y plane ($\Theta = \pi/2$), and we choose the values $\epsilon^2 = 0.025$ and $\phi_v = 0.01$.

Unbounded simple shear flow. We first gain intuition by discussing the simple case of an unbounded suspension in an imposed linear shear flow ($\mathbf{u} = \mathrm{Pe}_f y\hat{\mathbf{x}}$, $\boldsymbol{\omega} = -\mathrm{Pe}_f\hat{\mathbf{z}}$), a situation also recently analyzed by Vincenti *et al.* [37]. In this case, we define the intrinsic shear viscosity as

$$[\eta] = \lim_{\phi_v \to 0} \frac{\Sigma_{yx} - \mathrm{Pe}_f}{\phi_v \mathrm{Pe}_f}, \tag{12}$$

which takes on the simple form

$$[\eta] = \frac{5}{2} + \frac{3\beta}{\mathrm{Pe}_f}(\sin\Phi m_x - \cos\Phi\, m_y) + \frac{6\alpha}{\mathrm{Pe}_f} D_{yx}. \tag{13}$$

It is straightforward to realize that $[\eta](\Phi + \pi) = [\eta](\Phi)$, and therefore we only consider field orientations $\Phi \in [0, \pi]$. We also focus on the case of pushers for which $\alpha < 0$.

Results for the intrinsic viscosity are presented in fig. 2. In the absence of magnetic or active stresses, $[\eta] = 5/2$ due to the passive stresslet resulting from the enhanced dissipation around the particles [2]. When a magnetic field is applied, magnetic stresses can either enhance or decrease this value depending on the sign of $(\mathbf{m} \times \mathbf{h})_z = \sin\Phi m_x - \cos\Phi m_y$. Defining an angle $\Upsilon = \tan^{-1}(m_y/m_x)$, which captures the mean swimmer orientation, we see that $[\eta]$ is reduced by magnetic stresses whenever $\Phi < \Upsilon < \Phi + \pi$, and enhanced otherwise. In an applied shear flow, the applied field always resists particle rotations resulting in $\Phi - \pi < \Upsilon < \Phi$, and therefore $[\eta]$ monotonically increases with β as shown by the dashed lines in fig. 2(a). In the limit of strong fields, $[\eta]$ approaches 4 in agreement with previous predictions [33]. Active stresses, however, qualitatively modify this trend through the last term in eq. (13), which depends on the sign of D_{yx}. For fields nearly aligned with the flow direction ($\Phi \gtrsim 0$), particles tends to point in the fourth quadrant $-\pi/2 < \Upsilon < 0$ so that $D_{yx} < 0$ and $[\eta]$ is slightly enhanced for pushers ($\alpha < 0$). As Φ increases towards $\pi/2$, Υ enters the first extensional quadrant resulting in $D_{yx} > 0$ and in a decrease in viscosity, which reaches a minimum for a value of

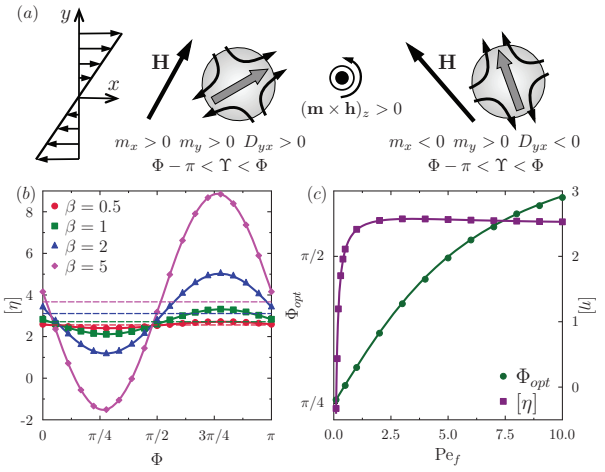

Fig. 2: (Color online) (a) Mean particle orientation and mechanism for viscosity modification in unbounded simple shear flow for two magnetic field orientations. Disturbance flow fields are shown for pushers and have the opposite direction for pullers. (b) Intrinsic viscosity $[\eta]$ for $\mathrm{Pe}_f = 0.5$ as a function of magnetic field direction Φ for varying field strengths β. Dashed lines: movers (no active stress, $\alpha = 0$). Solid lines: pushers ($\alpha = -5/3$), where the solution is also checked using spherical harmonics (symbols). (c) Optimum field direction Φ_{opt} (left axis), in a suspension of pushers, that minimizes $[\eta]$ (right axis) as a function of the flow Péclet number Pe_f. Results for pullers are obtained by noting $\Phi_{opt}(\alpha) = \Phi_{opt}(-\alpha) + \pi/2$. Solid line: analytical predictions of eqs. (14) and (17). Symbols: numerical solution.

$\Phi \approx \pi/4$ in weak flows. Further increasing Φ beyond $\pi/2$ causes particles to align in the second compressional quadrant, and thus $[\eta]$ is enhanced again. In stronger flows, similar trends are observed but require larger values of Φ to resist rotation in the applied flow. For the purpose of decreasing the intrinsic viscosity, fig. 2 suggests that an optimum field direction Φ_{opt} exists, which is also that maximizing D_{yx} in the case of pushers.

We seek analytical expressions for $[\eta]$ and Φ_{opt} by taking orientational moments of eq. (10) and applying a closure approximation for the third-order moment [20,28]. In an unbounded homogeneous suspension, this transformation reduces the conservation equation to a system of coupled algebraic equations for $\mathbf{m}$ and $\mathbf{D}$:

$$-\mathbf{W}\cdot\mathbf{m} + \beta\left(\frac{2}{3}\mathbf{h} - \mathbf{D}\cdot\mathbf{h}\right) = 2\mathbf{m},$$

$$\mathbf{D}\cdot\mathbf{W} - \mathbf{W}\cdot\mathbf{D} + \beta\left[\frac{3}{5}(\mathbf{mh}+\mathbf{hm}) - \frac{2}{5}(\mathbf{m}\cdot\mathbf{h})\mathbf{I}\right] = 6\mathbf{D}.$$

Inverting this system and inserting the solution into eq. (13) yields an expression for the intrinsic viscosity:

$$[\eta](\mathrm{Pe}_f, \alpha, \beta, \Phi) = P/Q, \tag{14}$$

where the functions P and Q are given by

$$P = \frac{375}{2}\left(\mathrm{Pe}_f^4 + 52\mathrm{Pe}_f^2 + 576\right) - 100\beta^2\left(\mathrm{Pe}_f^2 - 234\right) + 24\frac{\alpha\beta^2}{\mathrm{Pe}_f}\left[\left(3\beta^2 - \frac{5}{2}\mathrm{Pe}_f^2 + 60\right)\sin 2\Phi - 25\mathrm{Pe}_f\cos 2\Phi\right], \tag{15}$$

$$Q = 75\left(\mathrm{Pe}_f^4 + 52\mathrm{Pe}_f^2 + 576\right) - 80\beta^2\left(2\mathrm{Pe}_f^2 - 63\right) + 144\beta^4. \tag{16}$$

This prediction perfectly matches the numerical results of fig. 2(b), (c). The optimum field direction Φ_{opt} can then be obtained by straightforward minimization as

$$\Phi_{opt} = \frac{1}{2}\tan^{-1}\left[\frac{\frac{5}{2}\mathrm{Pe}_f^2 - 3\beta^2 - 60}{25\mathrm{Pe}_f}\right], \tag{17}$$

which increases from $\pi/4$ as flow strength increases and also matches numerical calculations in fig. 2(c). Equation (17) also provides the dependence of Φ_{opt} on magnetic field strength: for a given flow strength Pe_f, the optimum angle decreases as β increases. In the limit of strong fields and moderate flows, particles orient approximately along the field direction, yielding an optimum angle of $\Phi_{opt} \gtrsim \pi/4$.

Magnetoactive pumping in confinement. We now turn to the effects of confinement and first analyze the dynamics in the absence of any imposed flow ($\mathrm{Pe}_f = 0$). In this case, fluid motion is solely the result of magnetic and active stresses which can produce a net non-zero volumetric flow rate $\dot{Q}_v = \int_0^1 u_x(y)dy$ by a mechanism summarized in fig. 3(a). Symmetry of the problem allows us to only consider $\Phi \in [0, \pi/2]$. When $\beta = 0$ (no magnetic field), particles accumulate equally at both boundaries with a net polarization towards them [20,21], and no flow is generated ($\dot{Q}_v = 0$). Applying a magnetic field ($\beta > 0$) in any direction other than $\Phi = \pi/2$ results in a net torque on the particles, which competes against wall-induced polarization and is transmitted to the fluid via viscous drag. For a longitudinally applied field ($\Phi = 0$), the magnetic torque is clockwise ($\mathbf{m}\times\mathbf{h})_z < 0$ near the top wall and counter-clockwise near the bottom wall, and corresponding magnetic shear stresses drive a flow in the negative x-direction ($\dot{Q}_v < 0$). This is evident in fig. 3(b), showing $\dot{Q}_v$ as a function of β for movers ($\alpha = 0$). In weak to moderate fields, $|\dot{Q}_v|$ increases with β as longitudinal polarization m_x progressively increases from zero. In strong fields, however, magnetic alignment overcomes wall-induced polarization, leading to $m_y \to 0$ and therefore to a drop in magnetic stresses and flow rate. In this limit, wall accumulation becomes negligible as particles primarily swim in the field direction. The transition between the two regimes is marked by a maximum in flow rate occurring for $\beta \sim 2.0$–3.0. The coupling of wall-normal polarization with field alignment also results in nematic alignment [20] with $D_{yx} > 0$ near the top wall and < 0 near the bottom wall. In the case of pushers in fig. 3(c), the resulting active stress profile further promotes retrograde flow ($\dot{Q}_v < 0$) by a mechanism similar to that for the viscosity decrease observed in pressure-driven flows [7]. In the case of pullers, however, active stresses have the opposite sign and can dominate magnetic stresses to drive a net flow in the positive x-direction ($\dot{Q}_v > 0$) as seen in fig. 3(d).

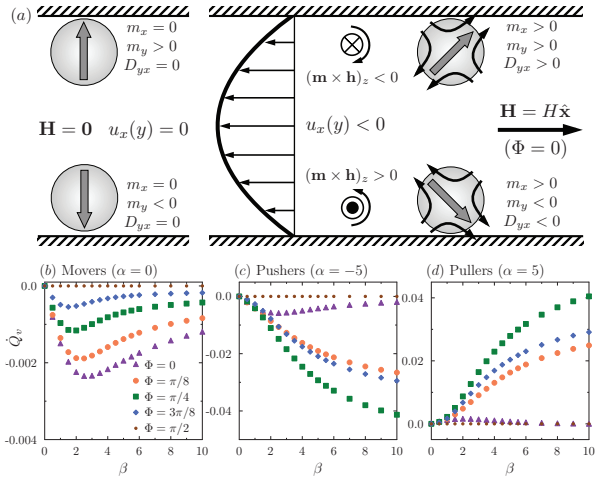

Fig. 3: (Color online) (a) Mechanism for magnetoactive pumping in a planar channel with no imposed flow ($\mathrm{Pe}_f = 0$). Left: average particle configuration in the absence of a magnetic field. Right: disturbance flow created by the synergistic effect of magnetic and active stresses in a suspension of pushers under a uniform magnetic field. In the case of pullers, magnetic stresses remain the same while active disturbance flows change sign. (b)–(d) Volumetric flow rate $\dot{Q}_v$ as a function of magnetic field strength β for $\mathrm{Pe}_s = 0.5$ and for different swimmer types: movers ($\alpha = 0$), pushers and pullers ($\alpha = \mp 5$).

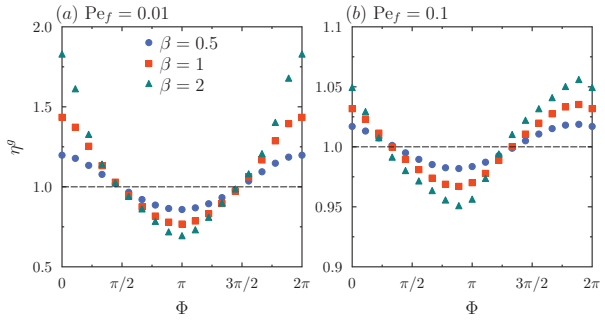

Fig. 4: (Color online) Dependence of the generalized Newtonian viscosity η^g on magnetic field direction Φ in a confined suspension of movers ($\alpha = 0$) subject to a linear shear flow: (a) $\mathrm{Pe}_f = 0.01$, (b) $\mathrm{Pe}_f = 0.1$. In both cases, $\mathrm{Pe}_s = 0.5$.

These basic trends on flow rate remain valid for non-parallel field directions ($\Phi > 0$). As Φ increases from zero, particle distributions become asymmetric with a stronger accumulation at the top wall; in sufficiently strong fields, accumulation at the lower boundary can be suppressed entirely, resulting in $m_y > 0$ throughout the channel. While the magnetically-driven flow rate monotonically decreases towards zero as Φ increases from 0 to $\pi/2$, as observed in fig. 3(b), activity-driven flows in both pusher and puller suspensions show a non-monotonic dependence, with a maximum $|\dot{Q}_v|$ attained for $\Phi \approx \pi/4$. Therefore, a transition between magnetically-dominated flows to activity-dominated flows manifests itself as $|\alpha|$ increases from zero. In the case of $\mathrm{Pe}_s = 0.5$ and $\beta = 2$, the transition occurs at a critical level of activity of $|\alpha_c| \approx 1$.

While these internally-driven active flows are reminiscent of the spontaneous unidirectional flows known to arise in confined suspensions of elongated pushers [8–10], a fundamental difference lies in the ability to turn flows on and off and control their strength and direction by tuning the magnetic field strength β and orientation Φ. We also note that particle accumulation at the boundaries as a result of swimming plays a crucial role in the mechanism of fig. 3(a): it is this very accumulation that induces polarization in the system, which upon application of the field generates both magnetic and active stress gradients.

Simple shear flow in confinement. Our understanding of unconfined rheology and of magnetoactive pumping in confinement provides the basis for analyzing the response in imposed confined flows. We first discuss the case of a linear shear flow between two planar walls, where the upper wall translates with constant velocity $u_w = \mathrm{Pe}_f$. Here, we define a generalized Newtonian viscosity

$$\eta^g = \frac{\mathrm{Pe}_f}{2\dot{Q}_v}, \tag{18}$$

which quantifies the change in volumetric flow rate $\dot{Q}_v$ due to the bacteria and reduces to 1 in the passive case.

Results for η^g in a weak imposed flow ($\mathrm{Pe}_f = 0.01$) are shown in fig. 4(a) for a suspension of movers ($\alpha = 0$). In this case, the flow has only a weak effect on particle configurations, which instead are controlled primarily by the interplay of magnetic alignment and wall-induced accumulation and polarization as was the case in fig. 3(a). Following the reasoning of the previous section, the resulting magnetic stress profile induces a disturbance flow in the direction opposite to the horizontal field component. It follows that magnetic stresses enhance the imposed flow for $\Phi \in [\pi/2, 3\pi/2]$ but impede it otherwise, resulting in an effective reduction in η^g in the latter case and increase otherwise, with a magnitude that increases with β. Pushers/pullers further enhance/mitigate this effect, respectively, as can be anticipated from fig. 3(c), (d).

In stronger flows, the applied shear affects the particle distribution more significantly and breaks the horizontal symmetry. This is illustrated in fig. 4(b) for $\mathrm{Pe}_f = 0.1$, where the leading effect of the flow is to substantially reduce departures of the generalized viscosity from unity. The hydrodynamic torque experienced by the particles acts in the clockwise direction across the entire channel; in a magnetic field, the mean particle orientation is position-dependent but tends to be such that $\Phi - \pi < \Upsilon < \Phi$ so that hydrodynamic and magnetic torques counteract each other. For small Φ, particles thus tend to swim towards and accumulate at the bottom wall, where the magnetic torque then acts to slow down the flow and therefore enhance viscosity. In order for η^g to be reduced, particle accumulation must be forced towards the upper wall where counterclockwise magnetic torques near the no-slip boundary tend to enhance the applied flow: this occurs

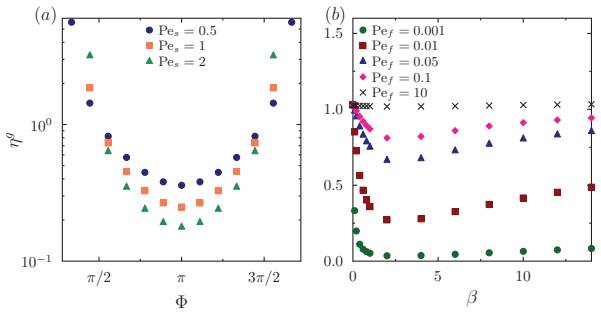

Fig. 5: (Color online) (a) Generalized viscosity η^g in a pressure-driven flow of movers ($\alpha = 0$) as a function of Φ for different values of Pe$_s$. Parameter values: Pe$_f = 0.01$, $\beta = 1$. (b) Dependence of η^g on magnetic field strength β for $\Phi = \pi$ and different values of Pe$_f$. Parameter values: Pe$_s = 0.5$, $\alpha = 0$.

for magnetic field orientations $\pi/4 \lesssim \Phi \lesssim 5\pi/4$ as seen in fig. 4(b). For yet higher angles Φ, particle accumulation returns to the lower wall and the effective viscosity η^g raises again above 1.

Pressure-driven flow in confinement. As a final example, we consider the effective rheology in a Poiseuille flow driven by a constant pressure gradient, which drives the flow from left to right. Here, we also introduce a generalized Newtonian viscosity

$$\eta^g = \frac{\mathrm{Pe}_f}{12\dot{Q}_v}, \tag{19}$$

which again reduces to 1 in the passive case. Results for η^g and its dependence on magnetic field direction are shown in fig. 5(a), where η^g is found to be reduced whenever $\pi/2 < \Phi < 3\pi/2$ and reaches a minimum for $\Phi = \pi$. This direction indeed maximizes the angle between $\mathbf{h}$ and $\mathbf{m}$, which directly controls the magnitude of magnetic stresses. The dependence of η^g on field strength for $\Phi = \pi$ is non-monotonic as shown in fig. 5(b), which is a result of changes in the distribution of particles across the channel. In weak fields, particles pointing towards the top/bottom walls feel a magnetic torque in the counterclockwise/clockwise directions, respectively, which is transmitted to the fluid and enhances the applied flow. This effective decrease in η^g becomes stronger with increasing β, up to a point where wall accumulation is suppressed as particle orientations become slaved to the field. This strong field alignment has two competing effects on the rheology. On the one hand, the weakening of accumulation causes a decrease in the passive viscous contribution to the stress, as fewer particles occupy the high-shear near-wall regions; this reduction in passive stress causes a further decrease of η^g. On the other hand, stronger alignment with the field also decreases magnetic stresses, which enhances the apparent viscosity. As β is increased, the second effect tends to dominate, which explains the eventual increase of η^g towards 1 in fig. 5(b). In very strong flows (Pe$_f = 10$), a qualitative change in particle

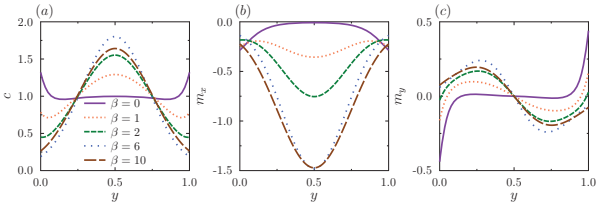

Fig. 6: (Color online) (a) Concentration, (b) streamwise and (c) transverse polarization in pressure-driven flow for a magnetic field oriented against the flow ($\Phi = \pi$). Parameter values: Pe$_s = 0.5$, $\alpha = 0$, Pe$_f = 10$.

Table 1: Cross-sectionally averaged fluid velocity $\overline{u}$ (μm/s) in magnetically-actuated flows, estimated based on typical experimental parameters [22].

		$\phi_v = 0.01$		$\phi_v = 0.1$	
Φ	α \ β	30	60	30	60
0	10	−0.05	−0.04	−0.35	−0.36
	100	0.66	0.15	4.96	1.20
	200	1.43	0.37	10.85	2.93
$\frac{\pi}{4}$	10	1.90	1.99	4.45	4.49
	100	19.04	19.91	42.10	43.04
	200	38.07	39.83	83.93	85.88

configurations is also observed, whereby particles now migrate towards the centerline of the channel (fig. 6). This magnetic focusing, which has previously been reported in experiments [22] and explained theoretically [24], causes a change in the sign of magnetic stresses as polarization now points towards the centerline; this has the effect of enhancing η^g and in fact causes it to exceed 1. The effect of varying flow strength is also illustrated in fig. 5(b), where shear-thickening is observed for all values of β, primarily as a consequence of passive stresses which become dominant in strong flows.

Experimental estimates. – We finish by providing numerical estimates for the magnitude of magnetically-actuated flows based on typical experimental parameters such as those of Waisbord *et al.* [22], who used *M. marinus* bacteria with radius $a \approx 1\,\mu$m, swimming speed $V_0 \approx 140\,\mu$m/s, rotational diffusivity $d_r \approx 0.5\,\mathrm{s}^{-1}$, and magnetic moment $M \approx 10^{-16}\,\mathrm{A}\cdot\mathrm{m}^2$. The value of σ_0 is unknown; we use the estimate of $\sigma_0 \approx 8 \times 10^{-19}\,\mathrm{N}\cdot\mathrm{m}$ obtained for *E. coli* [36] but consider puller swimmers which *M. marinus* is thought to be [22]. The channel width is taken to be $L = 50\,\mu$m. The corresponding dimensionless groups are Pe$_s = 5.6$, $\alpha = 200$ and $\epsilon^2 = 5 \times 10^{-4}$. This value of ϵ^2 results in exceedingly thin accumulation layers that are challenging to resolve numerically; we use $\epsilon^2 = 0.03$ instead in our calculations, which only weakly affects flow rate and viscosity. Finally, we consider two volume fractions $\phi_v = 0.01$ and 0.1, and two magnetic field strengths of $H = 1.75\,$mT and $3.5\,$mT corresponding to $\beta = 30$ and

60. Estimates for the cross-sectionally averaged fluid velocity $\overline{u}$ for these cases are provided in table 1. For weak levels of activity ($\alpha = 10$), the flow is dominated by magnetic stresses resulting in fairly weak negative velocities. As α increases, active stresses in puller suspensions change the flow direction and result in significantly larger velocities, especially for $\Phi = \pi/4$. Velocity magnitudes in these cases are on the order of tens of μm/s, which makes them relevant for microfluidic applications.

Concluding remarks. – We have used a continuum kinetic model to explore the use of magnetotactic bacterial suspensions as tunable active fluids whose rheological response in an external flow can be controlled by an applied magnetic field. In confined systems, we also demonstrated the ability of these fluids to internally drive steady unidirectional flows, whose strength and direction are easily adjusted by tuning the applied field. The role of particle activity in these systems was found to be twofold: i) firstly, active stresses generated by self-propulsion directly modify the rheology and can be harnessed in various ways by controlling particle orientations using the external field; ii) perhaps yet more interestingly, the wall accumulation resulting from self-propulsion in confined geometries induces local polarization, which under the action of the field gives rise to magnetic stresses whose sign can again be controlled. The richness of behaviors exhibited by these systems and the ability to externally control their rheological response and even to drive flows internally hold great promise for microfluidic and lab-on-a-chip applications requiring local flow actuation without moving parts. For such applications, the design of artificial suspensions of self-propelled nano-magnetic units may be desirable [23]. Our study also paves the way for analyzing the dynamics of more complex systems, such as semi-dilute suspensions where the role of active and magnetic stresses in driving large-scale instabilities [22] has yet to be elucidated.

* * *

We thank C. Cottin-Bizonne, I. Frankel, and C. Rinaldi for useful conversations. Support from NSF Grant DMS-1463965 is gratefully acknowledged.

REFERENCES

[1] Saintillan D., *Annu. Rev. Fluid Mech.*, **50** (2018) 563.
[2] Guazzelli E. and Morris J. F., *A Physical Introduction to Suspension Dynamics* (Cambridge University Press) 2012.
[3] Hatwalne Y., Ramaswamy S., Rao M. and Aditi Simha R., *Phys. Rev. Lett.*, **92** (2004) 118101.
[4] Gachelin J., Miño G., Berthet H., Lindner A., Rousselet A. and Clément E., *Phys. Rev. Lett.*, **110** (2013) 268103.
[5] López H. M., Gachelin J., Douarche C., Auradou H. and Clément E., *Phys. Rev. Lett.*, **115** (2015) 028301.
[6] Saintillan D., *Exp. Mech.*, **50** (2010) 1275.
[7] Alonso-Matilla R., Ezhilan B. and Saintillan D., *Biomicrofluidics*, **10** (2016) 043505.
[8] Wioland H., Lushi E. and Goldstein R. E., *New J. Phys.*, **18** (2015) 075002.
[9] Creppy A., Plouraboué F., Praud O., Druart X., Cazin S., Yu H. and Degond P., *J. R. Soc. Interface*, **13** (2016) 20160575.
[10] Theillard M., Alonso-Matilla R. and Saintillan D., *Soft Matter*, **13** (2017) 363.
[11] Sheng P. and Wen W., *Annu. Rev. Fluid Mech.*, **44** (2012) 143.
[12] de Vicente J., Klingenberg D. J. and Hidalgo-Alvarez R., *Soft Matter*, **7** (2011) 3701.
[13] McTague J. P., *J. Chem. Phys.*, **51** (1969) 133.
[14] Brenner H., *J. Colloid Interface Sci.*, **32** (1970) 141.
[15] Hall W. and Busenberg S., *J. Chem. Phys.*, **51** (1969) 137.
[16] Levi A., Hobson R. and McCourt F., *Can. J. Phys.*, **51** (1973) 180.
[17] Leal L., *J. Fluid Mech.*, **46** (1971) 395.
[18] He X., Elborai S., Kim D., Lee S.-H. and Zahn M., *J. Appl. Phys.*, **97** (2005) 10Q302.
[19] Blakemore R. P., *Science*, **190** (1975) 377.
[20] Ezhilan B. and Saintillan D., *J. Fluid Mech.*, **777** (2015) 482.
[21] Ezhilan B., Alonso-Matilla R. and Saintillan D., *J. Fluid Mech.*, **781** (2015) R4.
[22] Waisbord N., Lefèvre C. T., Bocquet L., Ybert C. and Cottin-Bizonne C., *Phys. Rev. Fluids*, **1** (2016) 053203.
[23] van Oene M. M., Dickinson L. E., Pedaci F., Köber M., Dulin D., Lipfert J. and Dekker N. H., *Phys. Rev. Lett.*, **114** (2015) 218301.
[24] Matsunaga D., Meng F., Zöttl A., Golestanian R. and Yeomans J. M., *Phys. Rev. Lett.*, **119** (2017) 198002.
[25] Lauga E. and Nadal F., *EPL*, **116** (2017) 64004.
[26] Meng F., Matsunaga D. and Golestanian R., arXiv:1710.08339v1 (2017).
[27] Frankel R. B., *Annu. Rev. Biophys. Bioeng.*, **13** (1984) 85.
[28] Saintillan D. and Shelley M. J., *C. R. Phys.*, **14** (2013) 497.
[29] Saintillan D. and Shelley M. J., *Theory of active suspensions*, in *Complex Fluids in Biological Systems* (Springer) 2015, pp. 319–355.
[30] Doi M. and Edwards S. F., *The Theory of Polymer Dynamics* (Oxford University Press) 1986.
[31] Kim S. and Karrila S. J., *Microhydrodynamics: Principles and Selected Applications* (Dover) 2005.
[32] Batchelor G., *J. Fluid Mech.*, **41** (1970) 545.
[33] Brenner H. and Weissman M. H., *J. Colloid Interface Sci.*, **41** (1972) 499.
[34] Jansons K. M., *J. Fluid Mech.*, **137** (1983) 187.
[35] Drescher K., Goldstein R. E., Michel N., Polin M. and Tuval I., *Phys. Rev. Lett.*, **105** (2010) 168101.
[36] Drescher K., Dunkel J., Cisneros L. H., Ganguly S. and Goldstein R. E., *Proc. Natl. Acad. Sci. U.S.A.*, **108** (2011) 10940.
[37] Vincenti B., Douarche C. and Clément E., to be published in *Phys. Rev. Fluids* (arXiv:1710.01954 (2017)).